Mon. Not. R. Astron. Soc. **412,** 2063–2070 (2011) doi:10.1111/j.1365-2966.2010.18039.x

Mid-infrared colour gradients and the colour–magnitude relation in Virgo early-type galaxies

M. S. Clemens,[1⋆] P. Panuzzo,[2] R. Rampazzo,[1] O. Vega[3] and A. Bressan[1,3,4⋆]

[1]*INAF-Osservatorio Astronomico di Padova, Vicolo dell'Osservatorio, 5, 35122 Padova, Italy*
[2]*CEA, Laboratoire AIM, Irfu/SAp, Orme des Merisiers, F-91191 Gif-sur-Yvette, France*
[3]*INAOE, Luis Enrique Erro 1, 72840 Tonantzintla, Puebla, Mexico*
[4]*SISSA-ISAS, International School for Advanced Studies, ia Beirut 4, 34014 Trieste, Italy*

Accepted 2010 November 16. Received 2010 October 18; in original form 2010 June 23

ABSTRACT

We make use of *Spitzer* imaging between 4 and 16 μm and near-infrared data at 2.2 μm to investigate the nature and distribution of the mid-infrared emission in a sample of early-type galaxies (ETGs) in the Virgo cluster. These data allow us to conclude, with some confidence, that the emission at 16 μm in passive ETGs is stellar in origin, consistent with previous work concluding that the excess mid-infrared emission comes from the dusty envelopes around evolved asymptotic giant branch (AGB) stars. There is little evidence for the mid-infrared emission of an unresolved central component, as might arise in the presence of a dusty torus associated with a low-luminosity active galactic nucleus.

We none the less find that the 16-μm emission is more centrally peaked than the near-infrared emission, implying a radial stellar population gradient. By comparing with independent evidence from studies at optical wavelengths, we conclude that a metallicity that falls with increasing radius is the principal driver of the observed gradient.

We also plot the mid-infrared colour–magnitude diagram and combine with similar work on the Coma cluster to define the colour–magnitude relation for absolute *K*-band magnitudes from −26 to −19. Because a correlation between mass and age would produce a relation with a gradient in the opposite sense to that observed, we conclude that the relation reflects the fact that passive ETGs of lower mass also have a lower average metallicity. The colour–magnitude relation is thus driven by metallicity effects.

In contrast to what is found in Coma, we do not find any objects with anomalously bright 16-μm emission relative to the colour–magnitude relation. Although there is little overlap in the mass ranges probed in the two clusters, this may suggest that observable 'rejuvenation' episodes are limited to intermediate-mass objects.

Key words: galaxies: clusters: general – galaxies: elliptical and lenticular cD – galaxies: evolution – galaxies: photometry – infrared: galaxies.

1 INTRODUCTION

The mid-infrared emission of even the most passive early-type galaxies (ETGs) shows an excess of emission longwards of ∼8 μm over that which is expected from purely photospheric emission. This excess emission was detected by Impey, Wynn-Williams & Becklin (1986) using ground-based observations and was subsequently studied using *Infrared Space Observatory* (*ISO*; e.g. Bressan et al. 2001). The excess has now been observed in the central regions of bright ETGs in the Virgo cluster (Bressan et al. 2006) using *Spitzer*-IRS. Although some ETGs show a mid-infrared excess that is evidently caused by warm dust in a star-forming interstellar medium (Panuzzo et al. 2007), the excess in passive objects can be explained as the integrated emission from the hot dust in the envelopes of evolved asymptotic giant branch (AGB) stars. However, hot dust emission could also arise from the dusty torus around a central active galactic nucleus (AGN) of low luminosity.

Although there is evidence that the emission at 16 μm is extended in Coma cluster galaxies (Clemens et al. 2009a), the weight of evidence for this is far from conclusive. In this paper, we discuss *Spitzer*-IRS peak-up imaging at 16 μm of ETGs in the Virgo cluster that permits the investigation of the spatial distribution of the

⋆E-mail: marcel.clemens@oapd.inaf.it (MSC); alessandro.bressan@oapd.inaf.it (AB)

excess mid-infrared emission. In order to isolate the effects of the mid-infrared excess caused by AGB stars, we also use infrared array camera (IRAC) images at 4.5 and 8.0 μm because these are relatively unaffected by the excess and sample the purely photospheric component at the longest possible wavelength. We will argue that the excess is stellar in origin, as has been previously suggested (Bressan, Granato & Silva 1998; Athey et al. 2002; Xilouris et al. 2004).

The stellar origin of the excess mid-infrared emission makes it a particularly useful age/metallicity diagnostic because the contribution of the mid-infrared excess to the integrated spectrum varies with age and metallicity in a different way to optical diagnostics (Bressan et al. 1998). As a stellar population gets younger and/or the metallicity *increases*, the mid-infrared excess increases. However, the optical Hβ index becomes larger (optical colours bluer) as the age decreases and/or the metallicity *decreases*. The opposite behaviour of optical indices (colours, narrow-band indices and spectral shape) and mid-IR excess with respect to age and metallicity variations means that the mid-infrared spectral region, in combination with optical data, can disentangle age–metallicity effects in ETGs. Mid-infrared observations, then, can provide *without the need of accurate modelling* the explanation of the origin of the colour–magnitude relation in clusters of galaxies. This can be understood by considering the two following extremes.

(i) If galaxies are coeval and the bluer colours towards the less luminous sources are due to lower average metallicity (e.g. Arimoto & Yoshii 1986), we expect the mid-infrared excess to become relatively less pronounced at decreasing luminosity.

(ii) If the galaxies have the same average metallicity and the bluer colours towards less luminous sources are due to a younger age (the alternative explanation allowed in principle by optical diagnostics), we expect the mid-infrared excess to become relatively more pronounced at decreasing luminosity.

Although most studies tend to find that both age and metallicity vary as a function of galaxy luminosity or velocity dispersion (e.g. Nelan et al. 2005; Thomas et al. 2005; Clemens et al. 2006, 2009b), it is not clear which is the main driver of the colour–magnitude relation in the cluster environment. Here we attempt to address this question using a multiwavelength approach.

In Clemens et al. (2009a), we used *Spitzer*-IRS peak-up imaging at 16 μm to populate the luminous part of the mid-infrared colour–magnitude diagram for the Coma cluster. In Coma, galaxies with K-band magnitudes only as faint as -22 could be studied. In this paper, we repeat the analysis for fainter objects in the Virgo cluster in order to extend the colour–magnitude relation to fainter magnitudes.

2 DATA ANALYSIS

The aperture photometry for both the IRAC and IRS peak-up images is based on post-basic calibration data (PBCD).

The 16-μm, blue peak-up images are background dominated and the background often shows fluctuations on spatial scales similar to the source sizes. Background-subtraction techniques that attempt to model the background as the smoothly varying component of an image thus either include extended emission from the galaxy as background or do not correct for the background fluctuations. This tends to cause an oversubtraction of the background in the vicinity of the galaxy. We therefore define the background level, at all wavelengths, to be the median value in an elliptical annulus, of width 1.5 pixels, centred on the galaxy, with semimajor axis and position angle as given by the mean optical diameter catalogued in 'Hyperleda'.[1] Thus we sample the background at twice the radius of the galaxy (see Fig. 1). This is actually the background estimation technique recommended for IRAC images of extended sources.[2]

Confusing sources, normally in the background, can be problematic, especially at 16 μm. For meaningful aperture photometry they need to be removed. In some cases, the contaminating sources were too close or bright to attempt removal (e.g. vcc 0951). In some cases, the 16-μm detections themselves were not at the catalogued position and so were taken as 'suspect' background sources and discarded (e.g. NGC 4366). For the remaining objects that showed nearby contaminating sources, we applied an algorithm to remove them which analysed the pixel distribution in a series of annuli with axial ratio and position angle equal to that of the galaxies. Pixels that deviated by more than a fixed number of standard deviations from the median value were replaced by the median value. The threshold for source removal was varied between two and four standard deviations and was sometimes applied iteratively to achieve the best results. In all cases, the results were carefully checked by eye.

Integrated fluxes were taken as the total flux within the background annulus. We stress that these fluxes are measured only for the purposes of determining the mean colour of the galaxies. Given the way in which the background is determined, they are not a good measure of the true integrated fluxes of the objects. The colours of the objects, however, should be robustly determined. When we come to plot the colour–magnitude diagram, we will use the total K-band magnitude of the galaxies as given in the Two Micron All Sky Survey (2MASS) catalogue, rather than our measurement from the 2MASS K-band image.

Radial colour profiles were determined using a series of elliptical annuli with axial ratios and position angles as given in 'Hyperleda'. Before fluxes were measured, the two images were first convolved to identical resolutions. This was achieved by convolving each image with the measured point spread function (PSF) of the other. For example, when considering the $K - [16]$ colour, the 2MASS K-band image was convolved with the *Spitzer* blue peak-up PSF and the 16-μm image was convolved with the 2MASS K-band PSF. Instrumental resolutions (FWHM) are 2.6, 1.7, 1.9 and 3.6 arcsec for 2MASS, IRAC 4.5 and 8 and 16 μm, respectively.

The error on the derived fluxes was taken as the quadrature sum of the rms variation within the aperture or annulus and the calibration error, which was taken as 5 per cent for the blue peak-up data and 10 per cent for the IRAC data (see the respective instrument handbooks).

All aperture photometry was performed using a custom pipeline written in IDL and use was made of the IDL Astronomy User's Library (Landsman 1995).

3 RESULTS

3.1 Contribution from a central point source in the mid-infrared?

Most ETGs in our sample show negative radial gradients in the $K - [16]$ colour, indicating that the mid-infrared 16-μm emission is more centrally concentrated than the K-band light. The IRS spectroscopy of Bressan et al. (2006) has already shown this emission to be extended. However, at 16 μm there are roughly similar contributions from the photospheric and dusty envelope components

[1] http://leda.univ-lyon1.fr

[2] http://ssc.spitzer.caltech.edu/irac/iracinstrumenthandbook/33/

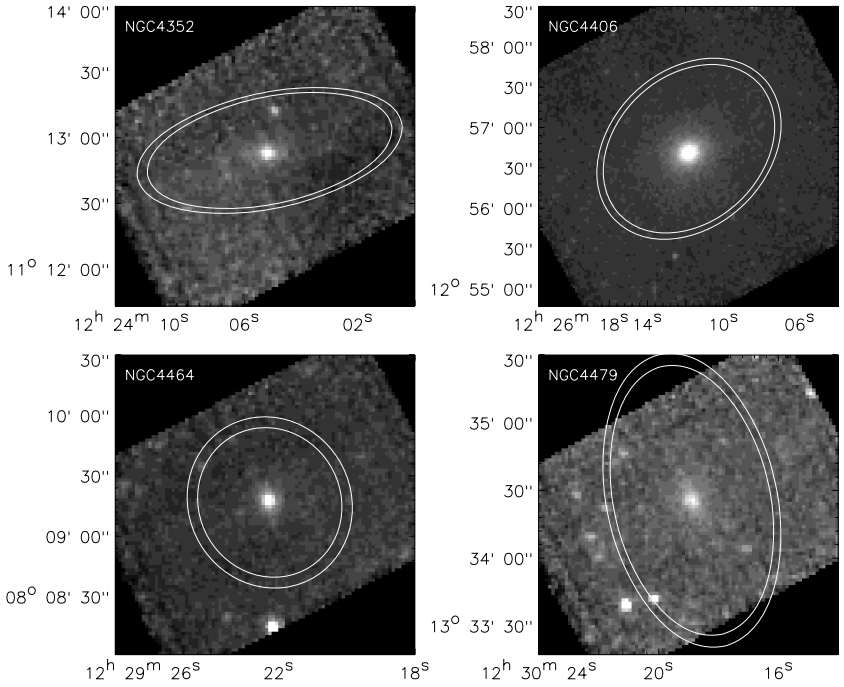

Figure 1. Example 16-μm images. The annuli used for the determination of the background are shown. Background sources that can be seen in some images were removed before the photometric measurements.

(See fig. 1 of Clemens et al. 2010), so it remains possible that only the stellar component is extended, while the dusty, *excess*, component is unresolved. This might be expected if these galaxies contained a dusty torus at their centre, associated with a low-luminosity AGN.

Using *Hubble Space Telescope* (*HST*) images, Carollo et al. (1997) interpreted the central dip in the optical surface brightness of NGC 4406 within 0.4 arcsec as evidence of a nuclear dust ring. NGC 4636 is classified as a LINER/Sy 3 and has radio jets at 1.4 and 4.8 GHz (Stanger & Warwick 1986). Both of these objects, then, show evidence of AGN activity. So is there any emission from a dusty torus at 16 μm?

Although Clemens et al. (2009a) found no evidence for central point sources at 16 μm for the galaxies of Coma, based on effective radii estimates, the spatial resolution was insufficient to investigate this possibility in detail.

In order to test this possibility, we created model 16-μm images based on the *K*-band images for the four large galaxies in our sample. We first convolved the *K*-band images to the same resolution as the observed 16-μm images, and then added a central point source in the form of the 16-μm PSF. We then measured the radial surface brightness profiles for point sources of various strengths and compared with the observed 16-μm profiles. The results are illustrated in Fig. 2.

We normalized the models in two different ways: first, to the observed surface brightness at a radius of 15 arcsec, so as to be far from any significant PSF effects and secondly, so that the observed central surface brightness was equal to that of the model with a 60 per cent contribution from a point source. The choice of 60 per cent is based on model fits to *Spitzer*-IRS profiles of passive ETGs that show that approximately this fraction of the 16-μm emission comes from the dusty circumstellar envelopes of AGB stars (Bressan et al. 2006). If the colour gradient is due to a population gradient involving AGB stars, then this would be a sensible upper limit to the extent to which the colour of the nucleus might differ from that at larger radii.

Fig. 2 shows that the observed profiles tend to have shallower gradients than one would expect if a central point source were the cause of the observed colour gradients. None the less, the limited signal-to-noise ratio and spatial resolution of the 16-μm images means that a central point source is permitted at some level. The most interesting case is NGC 4636 because this contains a radio-loud AGN. The observed profile in Fig. 2 is clearly much shallower than would be expected if there were a significant contribution from a central point source. At least for this galaxy, there is no evidence of a significant contribution to the mid-infrared emission from warm dust in a central torus. The observed colour gradient is therefore due to a stellar population gradient. If this is so for an ETG with a known AGN, there seems little evidence that the colour gradients in the other galaxies are due to anything else. A similar conclusion was actually reached for the mid-infrared emission of M 87, where the only excess over purely stellar emission is synchrotron emission from the radio-loud nucleus (Buson et al. 2009; Baes et al. 2010).

3.2 Radial colour gradients

Fig. 3 shows the radial mid-infrared colour profiles, $K - [4.5]$, $K - [8]$ and $K - [16]$. The signal-to-noise ratio of the 16-μm images limits the number of galaxies for which the $K - [16]$ colour profile can be plotted, and in general, profiles are truncated before noise becomes dominant. In addition, any objects that had nearby confusing sources have been excluded from the analysis. The four brightest galaxies are separated in the figure and have profiles that are well measured within a radius of ∼1 arcmin. We place more emphasis on these objects in the following discussion as the profiles are the most reliable.

For the four brightest objects, and for the majority of the fainter galaxies, at least at radii less than 10 arcsec, the $K - [16]$ colour

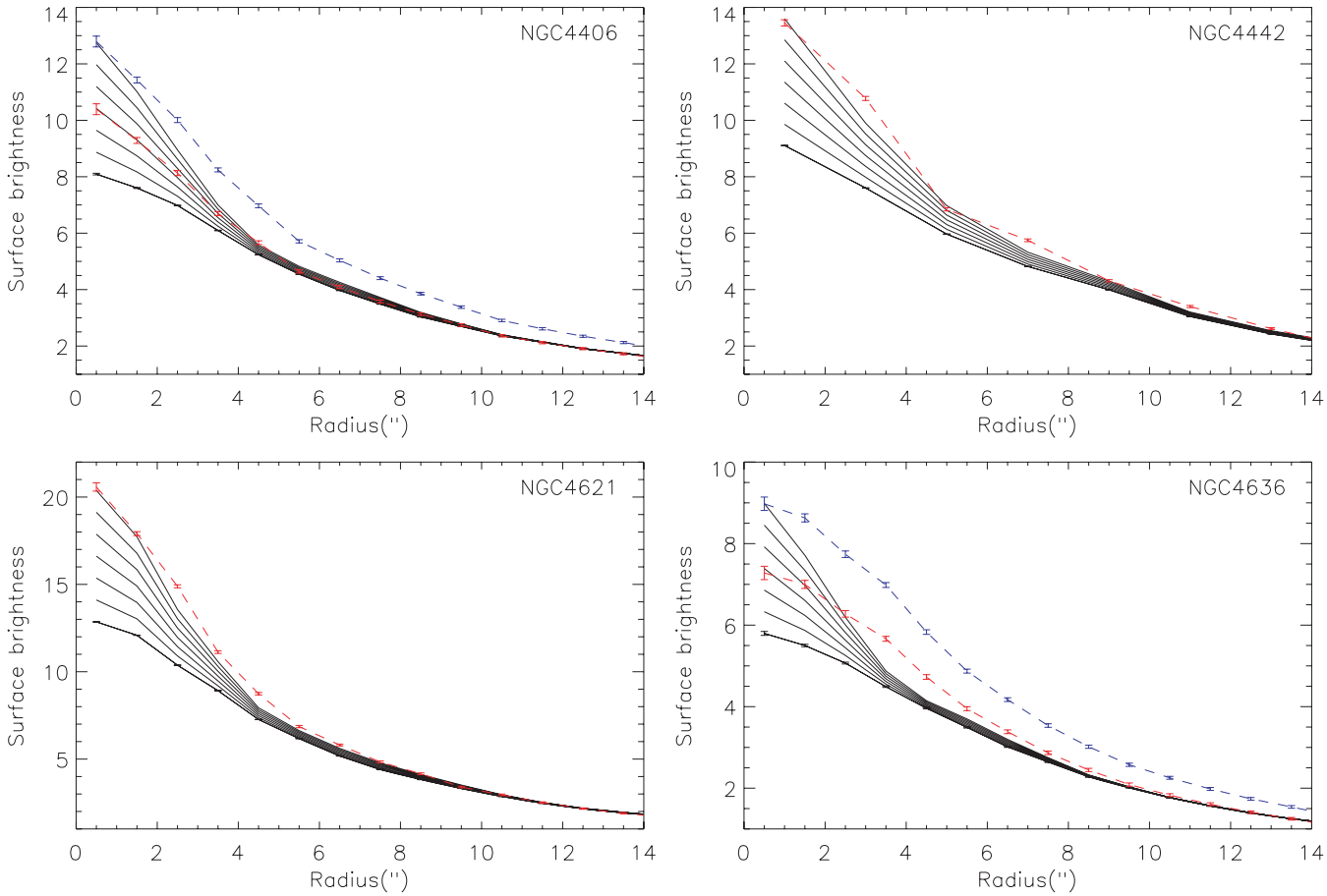

Figure 2. Comparison of model 16-μm surface brightness profiles (solid black lines) with the observed profiles for the four largest galaxies in the sample (dashed lines). For the red line, the models and observed profile have been normalized at a radius of 15 arcsec, well beyond any significant PSF effects. The blue line, instead, is normalized to a central point source contribution of 60 per cent, approximately the contribution of dusty AGB star envelopes as measured in *Spitzer*-IRS spectra. The model profiles assume a 16-μm brightness similar to that in the *K*-band with an additional point source at the centre. The contribution of the point source rises from zero (bottom line) in increments of 10 per cent. Surface brightness units are arbitrary.

shows a negative radial gradient that is steeper than that of either the $K - [4.5]$ or $K - [8]$ gradients. We also see that (with the exception of NGC 4516) the $K - [4.5]$ and $K - [8]$ profiles are very nearly parallel. In several cases, including the brightest galaxies, these profiles are almost flat.

With reference to the model fits to mid-infrared *Spitzer*-IRS spectra (Bressan et al. 2006), we expect both the 4.5- and 8-μm micron fluxes to be dominated by emission from stellar photospheres. However, at 16 μm this changes, with approximately 60 per cent of the emission coming from the hot dusty envelopes around evolved AGB stars. This offers a very natural explanation for the observed difference between the mid-infrared colour profiles, suggesting that the radial distribution of dusty AGB stars is more centrally concentrated than that of the general stellar population.

3.3 Colour–magnitude diagram

Table 1 gives the mid-infrared colours of our sample galaxies determined within the optical radius, as described in Section 2.

In Fig. 4, we show the mid-infrared colour–magnitude diagram for those Virgo galaxies for which the $K - [16]$ colour could be reliably determined. In light grey, we reproduce the values obtained for the Coma cluster by Clemens et al. (2009a). The galaxies observed in the Virgo cluster allow this diagram to be extended to fainter magnitudes than was possible for the Coma cluster alone, with objects down to an absolute *K*-band magnitude of −19.23.

The colour–magnitude relation of the Coma cluster showed a trend for bluer $K - [16]$ colours towards fainter magnitudes. The addition of the fainter Virgo galaxies shows that this trend continues to fainter magnitudes. There appears to be a slight offset between the Coma and Virgo data. Although this could be caused by an error in the relative distance of the two clusters (taken to be 97 and 17 Mpc, respectively), it may also be due to the fact that the colours were determined within larger apertures for the Coma cluster. The sense of the offset (Virgo objects appearing with slightly higher than expected $K - [16]$) is consistent with the colour gradients described in Section 3.2.

We also note that the four bright Virgo galaxies lie on the low boundary of values of $K - [16]$ found in the Coma cluster. There is no obvious data analysis effect that could have caused such a bias.

4 DISCUSSION

Both age and metallicity can affect the strength of the integrated 16-μm emission from the dusty envelopes of the AGB population. Younger stellar populations, for example, should have a larger contribution from dusty AGB stellar envelopes. However, in order to separate the effects of age and metallicity, we will compare our

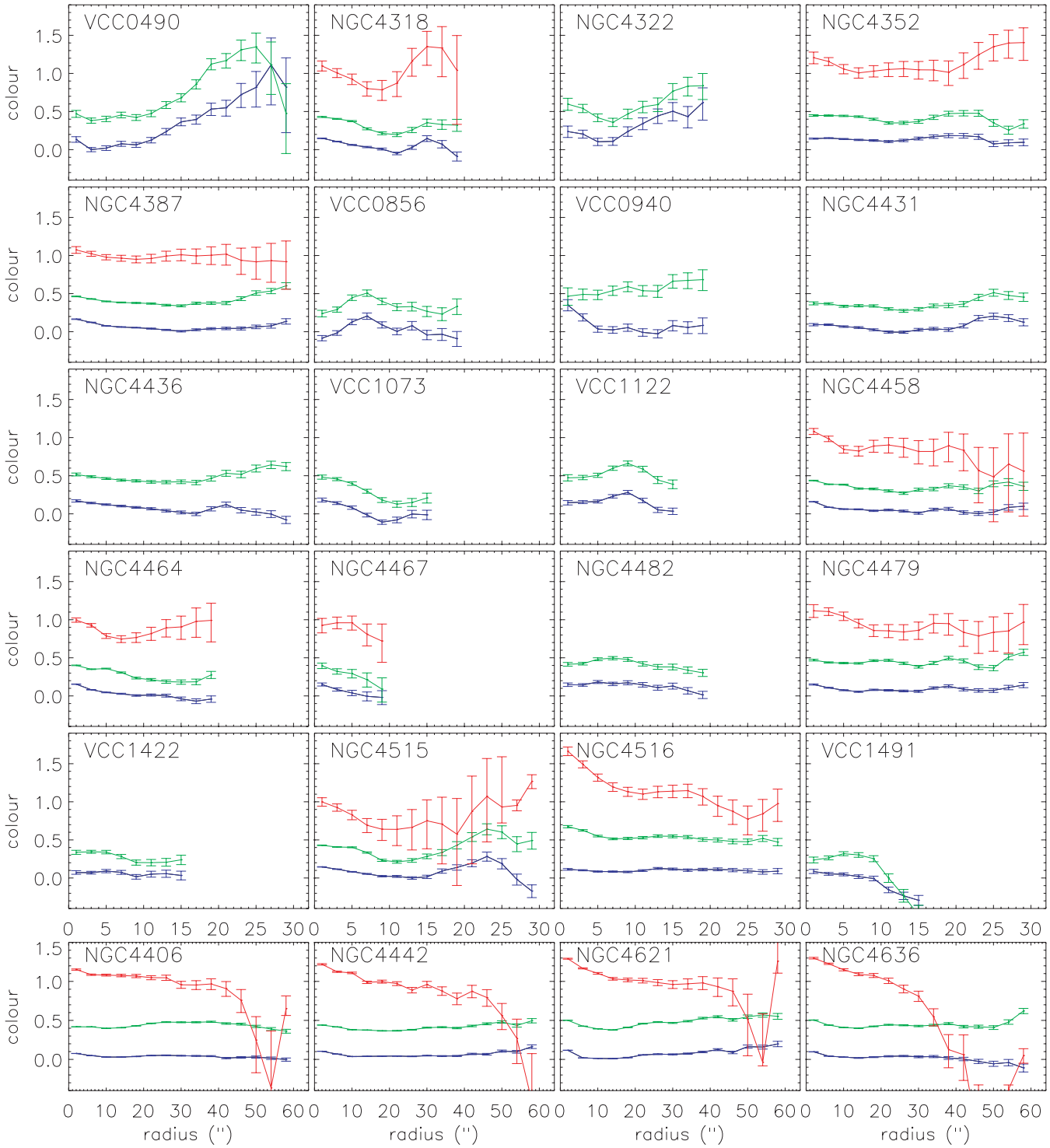

Figure 3. Mid-infrared radial colour profiles. Red: $K_s - [16]$; green: $K_s - [8]$; blue: $K_s - [4.5]$.

results with those of studies at optical wavelengths. As discussed in Section 1, the different responses of observables in the optical and infrared, to changes in metallicity and age, can be used to resolve the degeneracy between these two parameters.

4.1 Radial colour gradients

As discussed in Section 3.1, it seems likely that the radial gradients in the $K - [16]$ colour are due to a population gradient of AGB stars relative to the general stellar population. The redder $K - [16]$ colours towards the centre of the galaxies could be due to younger ages, higher metallicities or both.

Clemens et al. (2009b) have used optical line-strength indices of a sample of 14 000 ETGs from the Sloan Digital Sky Survey (SDSS) to determine age and metallicity as a function of mass, environment and also galactic radius. They find negative radial metallicity gradients for all masses. Although they also find positive radial age gradients for massive galaxies, this trend is less apparent

Table 1. Mean mid-infrared colours. Missing values imply either a non-detection in one band or that the source was confused. The errors in this table include the systematic calibration errors. These are not included in the error bars of Fig. 4.

Source ID	Type	K_s	$K_s - [4.5]$	$K_s - [8]$	$K_s - [16]$
vcc0490	dS0	−20.1	$0.15^{+0.104}_{-0.115}$	$0.51^{+0.105}_{-0.115}$	–
ngc4318	E	−21.2	$0.06^{+0.104}_{-0.114}$	$0.32^{+0.104}_{-0.115}$	$1.01^{+0.079}_{-0.086}$
ngc4322	dE	−19.4	$0.24^{+0.106}_{-0.117}$	$0.50^{+0.106}_{-0.118}$	–
ngc4352	S0	−21.4	$0.14^{+0.104}_{-0.115}$	$0.41^{+0.104}_{-0.115}$	$1.18^{+0.068}_{-0.073}$
ngc4366	dE	−19.8	–	–	–
vcc0786	dE	−19.2	$0.06^{+0.111}_{-0.122}$	$0.16^{+0.113}_{-0.125}$	–
ngc4387	E	−22.1	$0.07^{+0.104}_{-0.114}$	$0.41^{+0.104}_{-0.114}$	$0.94^{+0.065}_{-0.069}$
vcc0856	dE	−20.1	$0.07^{+0.105}_{-0.116}$	$0.37^{+0.105}_{-0.116}$	–
vcc0940	dE	−19.4	$0.05^{+0.105}_{-0.116}$	$0.54^{+0.107}_{-0.118}$	–
vcc0951	dE	−19.8	–	–	–
ngc4431	dS0	−20.9	$0.06^{+0.104}_{-0.115}$	$0.35^{+0.104}_{-0.115}$	$0.42^{+0.121}_{-0.137}$
ngc4436	dE	−20.5	$0.07^{+0.104}_{-0.115}$	$0.48^{+0.104}_{-0.115}$	–
vcc1073	dE	−20.4	$0.01^{+0.104}_{-0.115}$	$0.28^{+0.104}_{-0.115}$	$-0.13^{+0.217}_{-0.271}$
vcc1087	dE	−20.3	$0.14^{+0.143}_{-0.164}$	$0.38^{+0.255}_{-0.333}$	–
vcc1122	dE	−19.4	$0.14^{+0.104}_{-0.115}$	$0.51^{+0.104}_{-0.115}$	–
ngc4458	E	−21.8	$0.06^{+0.104}_{-0.114}$	$0.35^{+0.104}_{-0.115}$	$1.03^{+0.070}_{-0.075}$
ngc4464	E	−21.7	$0.04^{+0.104}_{-0.114}$	$0.30^{+0.104}_{-0.114}$	$0.81^{+0.063}_{-0.067}$
ngc4467	E	−20.2	$0.07^{+0.105}_{-0.116}$	$0.28^{+0.108}_{-0.120}$	$0.86^{+0.097}_{-0.106}$
vcc1254	dE	−20.1	$0.21^{+0.111}_{-0.122}$	$0.50^{+0.111}_{-0.122}$	–
ngc4482	dE	−20.7	$0.13^{+0.104}_{-0.115}$	$0.42^{+0.104}_{-0.115}$	$0.76^{+0.097}_{-0.106}$
ngc4479	S0	−21.5	$0.09^{+0.104}_{-0.114}$	$0.45^{+0.104}_{-0.115}$	$0.92^{+0.070}_{-0.075}$
vcc1308	dE	−18.5	$0.16^{+0.108}_{-0.119}$	$0.33^{+0.108}_{-0.120}$	–
vcc1348	dE	−18.6	–	–	–
vcc1422	E	−20.6	$0.06^{+0.104}_{-0.115}$	$0.27^{+0.104}_{-0.115}$	–
vcc1453	dE	−19.9	$0.15^{+0.104}_{-0.115}$	$0.46^{+0.104}_{-0.115}$	$0.08^{+0.256}_{-0.336}$
ngc4515	E	−21.3	$0.08^{+0.104}_{-0.114}$	$0.35^{+0.104}_{-0.115}$	$0.71^{+0.094}_{-0.103}$
ngc4516	S0	−21.4	$0.12^{+0.104}_{-0.114}$	$0.54^{+0.104}_{-0.115}$	$1.24^{+0.062}_{-0.066}$
vcc1491	dE	−19.2	$-0.01^{+0.104}_{-0.115}$	$0.21^{+0.104}_{-0.115}$	$-0.29^{+0.350}_{-0.520}$
ngc4406	E	−25.1	$0.04^{+0.103}_{-0.114}$	$0.43^{+0.103}_{-0.114}$	$1.02^{+0.054}_{-0.057}$
ngc4442	S0	−23.9	$0.06^{+0.103}_{-0.114}$	$0.40^{+0.103}_{-0.114}$	$0.96^{+0.054}_{-0.057}$
ngc4621	E	−24.5	$0.06^{+0.103}_{-0.114}$	$0.45^{+0.103}_{-0.114}$	$1.05^{+0.054}_{-0.057}$
ngc4636	E	−24.7	$0.03^{+0.104}_{-0.114}$	$0.44^{+0.104}_{-0.114}$	$0.93^{+0.055}_{-0.058}$

at intermediate masses and may even invert for low-mass galaxies. The four bright galaxies in our Virgo cluster sample have central velocity dispersions in the range 170–250 km s^{-1}. In this case, little or no age gradient is expected, at least on a statistical basis. Although it must be borne in mind that the results based on the SDSS are statistical in nature, and not necessarily applicable to any individual object, these results would favour metallicity effects over age effects as the cause of the mid-infrared colour gradients.

Negative metallicity gradients and negligible age gradients have, in fact, been found by other studies of ETGs both in the field (Annibali et al. 2007) and cluster (Peletier et al. 1999; Mehlert et al. 2003; Rawle et al. 2008) using optical line-strength indices.

4.2 Colour–magnitude relation

Since the work of Bower, Lucey & Ellis (1992), the colour–magnitude relation (its slope and narrowness) has been open to two interpretations. One is that ETGs are all very old and the slope of the colour–magnitude relation reflects a trend for lower mass galaxies to be less metal rich. The narrowness results from a small dispersion in the formation epoch with respect to the age of the system. In the second interpretation, if the luminosity-weighted 'average age' is allowed to vary, the only way to maintain a small dispersion is to invoke a synchronization mechanism, in such a way that lower mass ETGs appear younger.

For many years, the metallicity trend had been favoured partly because of its simplicity and partly because of lack of evidence for a relation between mass and age (e.g. Kodama et al. 1998). However, recently, numerous studies have found evidence for a so-called 'downsizing' effect (e.g. Cimatti, Daddi & Renzini 2006), which is nothing less than such a relation, in the sense that star formation is more prolonged in galaxies of lower mass. The evidence of the presence of a mechanism that links the mean age of an object to its mass restores some of the original doubt concerning the cause of the narrow colour–magnitude relation.

Studies at optical wavelengths, based on line-strength indices, find that less-massive galaxies tend to be younger and less metal rich (Bressan, Chiosi & Tantalo 1996; Kuntschner et al. 2001; Nelan

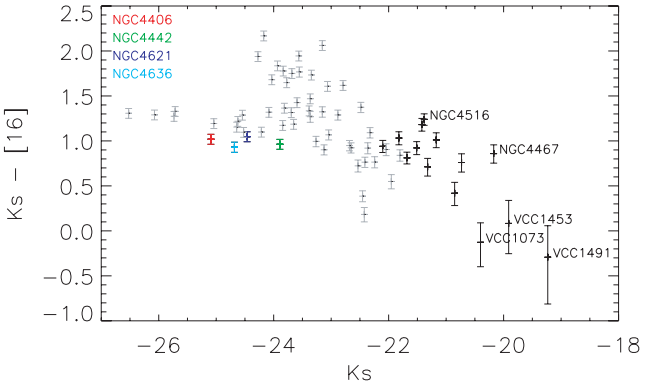

Figure 4. MIR colour–magnitude diagram. The colours are defined as those within 80 per cent of the optical radius given in 'Hyperleda'. K-band fluxes were taken from the 2MASS All Sky Survey.

et al. 2005; Thomas et al. 2005; Clemens et al. 2006; Smith, Lucey & Hudson 2007), both in the field and in the cluster environment. If the age trend holds also for the galaxies in our sample (both in Virgo and in Coma), then for a fixed metallicity, we would expect lower mass galaxies to have more 16-μm emission per K-band flux relative to the more massive objects, because of the greater importance of the dusty AGB phase, that is, low-luminosity objects should have higher values of $K - [16]$ if age were the dominant effect. The observed colour–magnitude relation, however, shows the opposite trend, with lower mass systems having lower $K - [16]$ colours. Metallicity, then, drives the mid-infrared colour–magnitude relation such that stellar populations with lower metallicity emit less 16-μm flux per unit stellar mass than their more metal-rich and more massive counterparts. In addition, population synthesis modelling of the $K - [16]$ versus $V - K$ colour plane shows that the optical colour–magnitude relation is also driven by a dominant metallicity effect (see fig. 6 of Clemens et al. 2009a). Thus, *Spitzer* shows that the cluster colour–magnitude relation is a sequence of metallicity rather than age.

Therefore, although a relation between mass and age could exist for our sample galaxies, this effect is dominated by a mass–metallicity trend that defines the colour–magnitude relation. Thus, 'downsizing', if present, is of secondary importance in passive ETGs.

The colour–magnitude diagram of the Coma cluster shows several objects that have high 16-μm fluxes relative to the colour–magnitude relation. None of the ETGs in the present Virgo sample shows this. Although the statistics are rather poorer for the Virgo sample and in Virgo we do not sample the luminosity range where these anomalous colours are seen in Coma, this may none the less indicate that the rejuvenation events that can be detected in the mid-infrared due to the increased 16-μm emission are limited to intermediate-mass objects.

5 CONCLUSIONS

We have observed a sample of low-luminosity ETGs in the Virgo cluster using the blue peak-up detector of *Spitzer*-IRS. Our aperture photometry of the spatially resolved images can be used to draw the following conclusions.

(i) The 16-μm emission that is in excess of that from stellar photospheres is extended. This emission is therefore consistent with an association with the dusty circumstellar envelopes around evolved AGB stars, rather than from a dusty torus around a low-luminosity AGN. This is a more robust conclusion than earlier evidence based on *Spitzer*-IRS spectroscopy (Bressan et al. 2006).

(ii) Mid-infrared colour gradients tend to show that the 16-μm emission is more centrally concentrated than the K-band light. Much shallower colour gradients involving bands dominated by photospheric emission, $K - [4.5]$ and $K - [8]$, imply a population gradient in the AGB stellar population. Comparison with independent studies at optical wavelengths implies that this is a metallicity effect.

(iii) The mid-infrared colour–magnitude relation, that we define over 8 mag by combining with similar data for the Coma cluster, is driven by metallicity. Less-massive objects are less metal rich.

(iv) If there is a relation between galaxy mass and age in these clusters, the effect is masked by the dominant metallicity effect. Thus, the mid-infrared colour–magnitude relation, together with optical studies, shows no evidence for so-called 'downsizing' in the cluster environment.

(v) The lack of objects with $K - [16]$ colours that place them well above the colour–magnitude relation of passive ETGs in the present Virgo sample, and for the most massive objects in the Coma sample of Clemens et al. (2009a), may be evidence that observable rejuvenation episodes are limited to intermediate-mass objects.

ACKNOWLEDGMENTS

MSC, AB and RR acknowledge support from contract ASI/INAF I/016/07/0.

We acknowledge the usage of the HyperLeda database (http://leda.univ-lyon1.fr).

This work is based on observations made with the *Spitzer Space Telescope*, which is operated by the JPL, Caltech under a contract with NASA.

We make use of data products from the 2MASS, which is a joint project of the University of Massachusetts and the Infrared Processing and Analysis Center/California Institute of Technology, funded by the National Aeronautics and Space Administration and the National Science Foundation.

This research has made use of the GOLD Mine Database.

REFERENCES

Annibali F., Bressan A., Rampazzo R., Zeilinger W. W., Danese L., 2007, A&A, 463, 455
Arimoto N., Yoshii Y., 1986, A&A, 164, 260
Athey A., Bregman J., Bregman J., Temi P., Sauvage M., 2002, ApJ, 571, 272
Baes M. et al., 2010, A&A, 518, L53
Bower R. G., Lucey J. R., Ellis R. S., 1992, MNRAS, 254, 601
Bressan A., Chiosi C., Tantalo R., 1996, A&A, 311, 425
Bressan A., Granato G. L., Silva L., 1998, A&A, 332, 135
Bressan A., Aussel H., Granato G.-L., Rodighiero G., Panuzzo P., Silva L., 2001, ApSSS, 277, 251
Bressan A. et al., 2006, ApJ, 639, L55
Buson L. et al., 2009, ApJ, 705, 356
Carollo C. M., Franx M., Illingworth G. D., Forbes D. A., 1997, ApJ, 481, 710
Cimatti A., Daddi E., Renzini A., 2006, A&A, 453, L29
Clemens M. S., Bressan A., Nikolic B., Alexander P., Annibali F., Rampazzo R., 2006, MNRAS, 370, 702
Clemens M. S., Bressan A., Panuzzo P., Rampazzo R., Silva L., Buson L., Granato G. L., 2009a, MNRAS, 392, 982
Clemens M. S., Bressan A., Nikolic B., Rampazzo R., 2009b, MNRAS, 392, L35
Clemens M. S. et al., 2010, A&A, 518, L50

Impey C. D., Wynn-Williams C. G., Becklin E. E., 1986, ApJ, 309, 572
Kodama T., Arimoto N., Barger A. J., Arag'on-Salamanca A., 1998, A&A, 334, 99
Kuntschner H., Lucey J. R., Smith R. J., Hudson M. J., Davies R. L., 2001, MNRAS, 323, 615
Landsman W. B., 1995, in Shaw R. A., Payne H. E., Hayes J. J. E., eds, ASP Conf. Ser. Vol. 77, Astronomical Data Analysis Software and Systems IV. Astron. Soc. Pac., San Francisco, p. 437
Mehlert D., Thomas D., Saglia R. P., Bender R., Wegner G., 2003, A&A, 407, 423
Nelan J. E., Smith R. J., Hudson M. J., Wegner G. A., Lucey J. R., Moore S. A. W., Quinney S. J., Suntzeff N. B., 2005, ApJ, 632, 137
Panuzzo P. et al., 2007, ApJ, 656, 206
Peletier R. F., Vazdekis A., Arribas S., del Burgo C., García-Lorenzo B., Gutiérrez C., Mediavilla E., Prada F., 1999, MNRAS, 310, 863
Rawle T. D., Smith R. J., Lucey J. R., Swinbank A. M., 2008, MNRAS, 389, 1891
Smith R. J., Lucey J. R., Hudson M. J., 2007, MNRAS, 381, 1035
Stanger V. J., Warwick R. S., 1986, MNRAS, 220, 363
Thomas D., Maraston C., Bender R., Mendes de Oliveira C., 2005, ApJ, 621, 673
Xilouris E. M., Madden S. C., Galliano F., Vigroux L., Sauvage M., 2004, A&A, 416, 41

This paper has been typeset from a TEX/LATEX file prepared by the author.